

Characterizing dielectric properties of ultra-thin films using superconducting coplanar microwave resonators

Nikolaj G. Ebensperger,¹ Benedikt Ferdinand,² Dieter Koelle,² Reinhold Kleiner,² Martin Dressel,¹ and Marc Scheffler^{1, a)}

¹⁾ *Physikalisches Institut, Universität Stuttgart, D-70569 Stuttgart, Germany*

²⁾ *Physikalisches Institut and Center for Quantum Science in LISA⁺, Universität Tübingen, D-72076 Tübingen, Germany*

(Dated: 1 November 2019)

We present an experimental approach for cryogenic dielectric measurements on ultra-thin insulating films. Based on a coplanar microwave waveguide design we implement superconducting quarter-wave resonators with inductive coupling, which allows us to determine the real part ε_1 of the dielectric function at GHz frequencies and for sample thicknesses down to a few nm. We perform simulations to optimize resonator coupling and sensitivity, and we demonstrate the possibility to quantify ε_1 with a conformal mapping technique in a wide sample-thickness and ε_1 -regime. Experimentally we determine ε_1 for various thin-film samples (photoresist, MgF₂, and SiO₂) in the thickness regime of nm up to μm . We find good correspondence with nominative values and we identify the precision of the film thickness as our predominant error source. Additionally we present a temperature-dependent measurement for a SrTiO₃ bulk sample, using an in-situ reference method to compensate for the temperature dependence of the superconducting resonator properties.

I. INTRODUCTION

The dielectric properties of insulating solids play a key role for technical applications^{1,2} as well as for fundamental research that addresses the underlying electronic properties of materials, which can be as diverse as band insulators, ferroelectrics, multiferroics, glasses, or other disordered materials^{3–6}. Therefore, various experimental techniques have been established to determine the dielectric function ε of sample materials. These techniques can differ strongly, depending on the particular sample (e.g. bulk vs. thin film) and physics of interest (e.g. relevant frequency and temperature ranges)^{7–13}. The goal of this work is to establish a technique to measure ε of ultra-thin films (down to a few nm) at cryogenic temperatures. The films are deposited onto dielectric substrates, and after film deposition no additional device processing shall be performed. As particular motivation we have in mind the experimental characterization of unconventional insulating states that occur in certain two-dimensional or strongly disordered electron systems at cryogenic temperatures down to the mK regime^{14–18}.

Our approach utilizes superconducting coplanar microwave resonators which fulfill our requirements concerning layout and sensitivity. They operate at GHz frequencies, which for such particular materials with characteristic energies of the scale of 1 K ($\approx 100 \mu\text{eV}$) either is well in the low-frequency (static) limit or reaches frequencies that match the fundamental energy and frequency scales of interest^{5,19,20}. For these experiments we profit from the vast existing experience concerning cryogenic planar microwave devices and in particular superconducting resonators^{21–24}, which are well established in the fields of superconductivity research^{25–27}, quan-

tum information^{28–30}, cryogenic detectors^{31–33}, and microwave spectroscopy^{20,34,35}.

II. MEASUREMENT PRINCIPLE AND SIMULATIONS

In this study we employ microwave waveguides in a coplanar geometry, which gives the straightforward possibility to address thin-film samples. A schematic cross-section of such a coplanar microwave waveguide is shown in Fig. 1(a), with its topography measured by atomic force microscopy (AFM). It consists of a 300 nm thick sputtered Nb film on top of a substrate, which we chose to be sapphire (Al₂O₃) due to its low microwave losses^{36–38}. Using optical lithography, an inner conductor as well as ground planes are patterned into the Nb film, which create an effective TEM-waveguide for the transmitted microwaves³⁹. The width S of the inner conductor and the distance W between inner conductor and ground planes have a constant ratio of about $S/W = 2.4$, thus matching the waveguide impedance to a nominal value of 50Ω of conventional microwave circuitry. Smaller W means higher sensitivity to the thin-film properties, but for reliable and reproducible fabrication we chose $W = 10 \mu\text{m}$ and $S = 24 \mu\text{m}$.

The inner conductor of the resonator is shaped in a meander-like structure with a total length l , as depicted in the top-view Fig. 1(c). It is coupled via a parallel arm of length l_c to a transmission line, the feedline, shown in red color. Such a feedline allows multiplexing several different resonators on the same chip^{31,33,40,41} located at different locations, as shown in Fig. 1(d). Each resonator can have a different length, this way we can vary its frequency. The end of each resonator near the feedline is closed, whereas the opposite end is connected to the ground planes and forms an open end. This combination leads to quarter-wave resonators carrying a standing wave³⁹.

^{a)} Electronic mail: scheffl@pi1.physik.uni-stuttgart.de

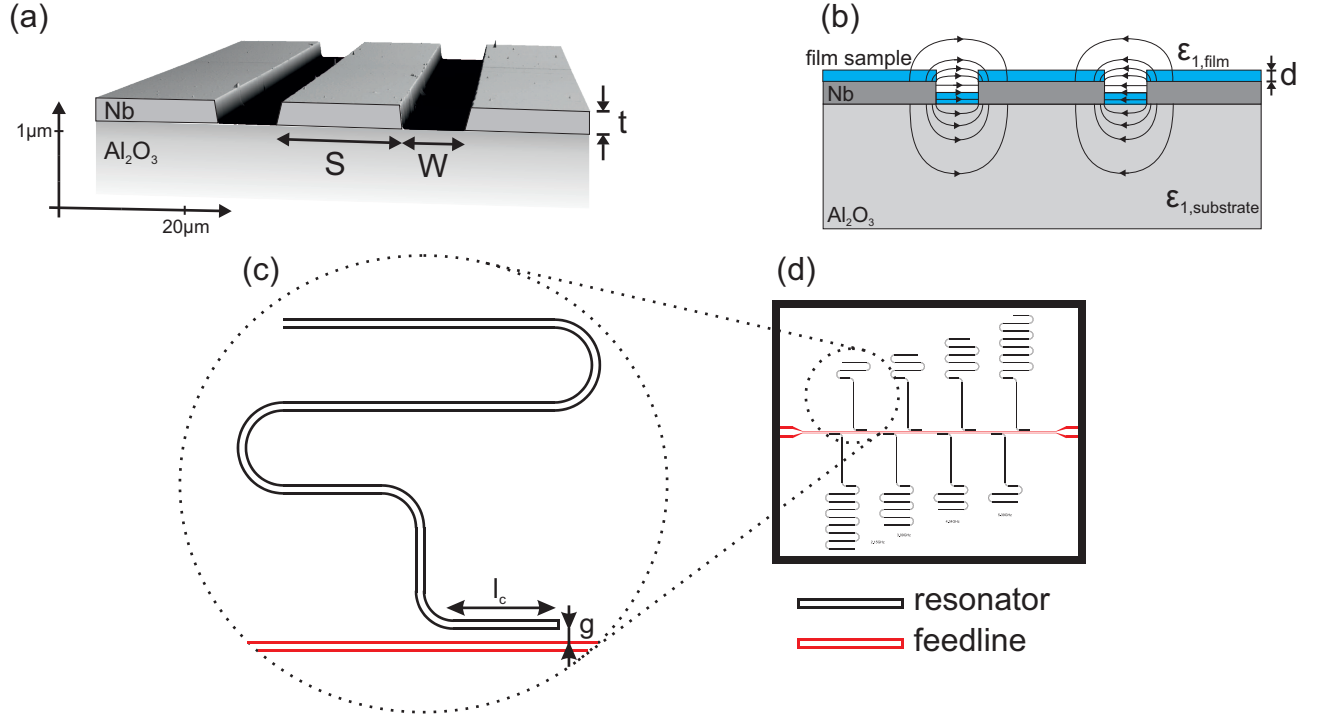


FIG. 1. (a) Atomic force microscope (AFM) measurement of the surface topography of a coplanar waveguide, combined with schematic cross-section. The Nb layer with thickness t on top of an Al_2O_3 substrate is structured as an inner conductor of width S and ground planes separated from the inner conductor by a gap of size W . The vertical scale is enhanced for clarity. (b) Schematic cross-section of a coplanar waveguide with applied thin-film sample layer with thickness d shown in blue. (c) Schematic top view of a $\lambda/4$ -resonator coupled inductively to the feedline. (d) Resonator chip consisting of the feedline with several multiplexed $\lambda/4$ -resonators. The resonator chip in total has eight resonators arranged to both sides of the feedline.

A. Simulations of empty resonator

The coupling strength between resonator and feedline is mainly determined by l_c and the distance g of the coupling arm to the feedline (compare Fig. 1(c)). Both quantities can be optimized to achieve sufficiently large excitation on the one hand, while on the other hand leaving the resonator undercoupled, such that the losses in the resonator are dominated by internal resonator properties^{22,42}. To find the optimal parameters we used the simulation software CST Microwave Studio. By simulating a three-dimensional model of one of our resonators we determined the microwave transmission parameter S_{21} of the signal passing the feedline, which features a dip at the resonance frequencies of the resonator as shown in Fig. 2(a). With a Lorentzian fit to these data, we can determine the resonance frequency ν_0 , the width of the resonance $\Delta\nu$ and consequently its quality factor $Q = \nu_0/\Delta\nu$. We also define the excitation strength of the resonator $1 - S_{21}(\nu_0)$ as the difference of the S_{21} -parameter at the resonance frequency ν_0 from total transmission (where $S_{21} = 1$). Varying l_c and g leads to changes in Q and in the excitation strength $1 - S_{21}(\nu_0)$ as shown in Fig. 2(b) and (c) for an exemplary 6.3 GHz resonance. With smaller l_c the coupling reduces, leading to a decrease in absorption at the resonance frequency (meaning weaker excitation of the resonator). However, the quality factor Q increases, showing that the resonator eventually becomes undercoupled⁴². For experimental applications it is necessary that the res-

onator is as much undercoupled as possible in order to be influenced primarily by the sample, while still retaining acceptable signal-to-noise ratio.

Since we expect some samples to introduce substantial losses into our measurements, we will use resonators with a decent amount of coupling, enhancing the signal-to-noise ratio but ultimately sacrificing some Q . For this we found reasonable values of $l_c = 400\mu\text{m}$ and $g = 10\mu\text{m}$, as determined from Fig. 2(b) and (c). Here, the strength of the excitation is already pretty high, while Q is still about 70 % of its maximum value.

B. Simulations of resonator with sample

Fig. 1(b) displays the cross-section of a coplanar waveguide with thin-film sample of thickness d deposited onto the resonator device. The propagating microwaves, with their electric field component schematically indicated as arrows in the figure, penetrate both the substrate as well as the thin-film sample. Their respective dielectric constants, $\epsilon_{1,\text{substrate}}$ and $\epsilon_{1,\text{film}}$, then have direct influence on the microwave propagation speed. The resonance frequencies of the resonators follow

$$\nu_0 = \frac{nc}{4l\sqrt{\epsilon_{\text{eff}}}}, \quad (1)$$

with l the length of the resonator, ϵ_{eff} the effective dielectric constant, c the vacuum speed of light and $n = 1, 3, 5, \dots$ the integer of the harmonic resonance

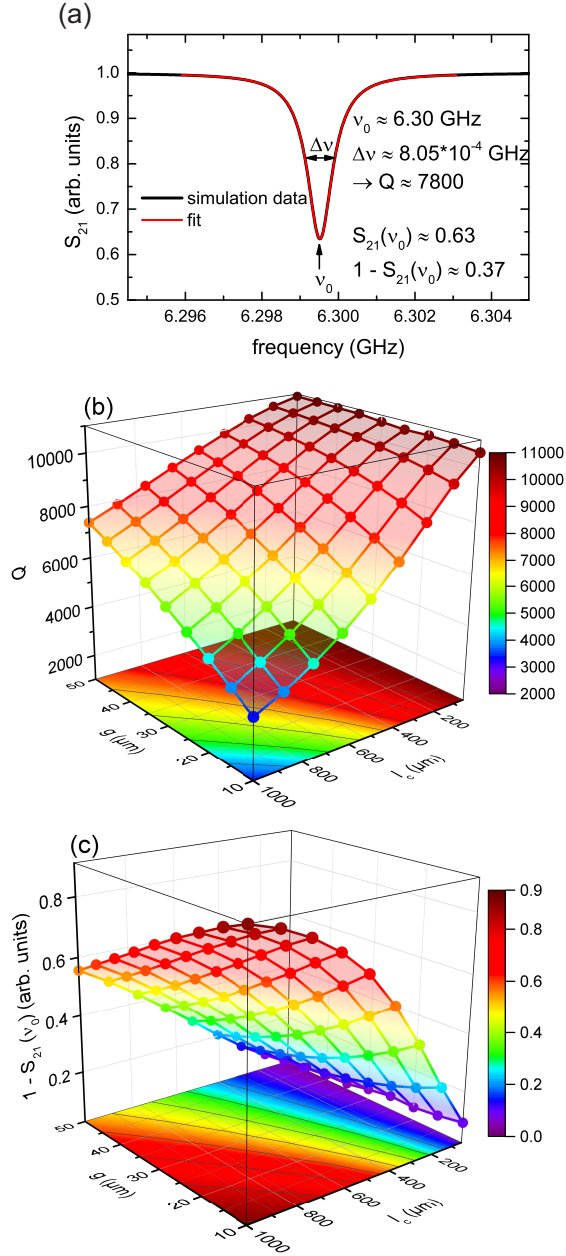


FIG. 2. (a) Simulated spectrum of a resonance at about 6.3 GHz, fitted with a Lorentzian. Characteristic parameters are shown. (b,c) Simulation data of (b) the quality factor Q and (c) the excitation strength $1 - S_{21}(\nu_0)$ for the resonance of a resonator at about 6.3 GHz as a function of the coupling arm length l_c and the distance of the resonator to the feedline g . With increasing l_c and decreasing g , that is with increasing coupling strength, Q decreases and $1 - S_{21}(\nu_0)$ increases.

with $n = 1$ the fundamental. The effective dielectric constant in turn is derived using the conformal mapping technique³⁹ as

$$\varepsilon_{\text{eff}} = \sum_i q_i \varepsilon_{1,i}, \quad (2)$$

with q_i the filling factor of the electromagnetic wave into the respective layer i and $\varepsilon_{1,i}$ the dielectric constant of the layer. For an empty resonator, consisting only of the Al_2O_3 -substrate with $\varepsilon_{1,\text{Al}_2\text{O}_3} \approx 10$ and the conductive

layer, this gives about $\varepsilon_{\text{eff}} \approx 5.5$. With a sample layer on top of the conductive layer, as shown in Fig. 1(b), this value increases accordingly.

In order to evaluate whether conformal mapping technique is appropriate for our experimental method, we performed simulations with a thin sample layer on top of a coplanar resonator. We varied both the thickness d of the sample layer and its dielectric constant $\varepsilon_{1,\text{film}}$. The resulting resonance frequency shift is shown in Fig. 3. At a certain thickness d (Fig. 3(c)) the resonance frequency ν shifts to lower frequencies upon increasing $\varepsilon_{1,\text{film}}$ from vacuum values ($\varepsilon_{1,\text{film}} = 1$), in this study to values of $\varepsilon_{1,\text{film}} \approx 300$. It follows an almost linear decrease, which can be compared with theory derived from conformal mapping in Eq. (2) and (1), shown as solid lines in the figure. These calculated values match the simulated data very well. Respectively, upon increasing the thickness d of the layer with fixed $\varepsilon_{1,\text{film}}$, ν also shifts to lower values (Fig. 3(a)). Here, an initial almost linear decrease (Fig. 3(b)) is followed by a saturation of ν at values larger than about $d \approx 10 - 20 \mu\text{m}$, which roughly corresponds to the dimensions of the resonator geometry ($S = 24 \mu\text{m}$ and $W = 10 \mu\text{m}$) and indicates that at larger thicknesses the sample can be considered bulk. Depending on $\varepsilon_{1,\text{film}}$ it saturates at different ν and corresponds to the expected resonance shift of a bulk sample. The theoretical predictions derived from conformal mapping (solid lines) again indicate very good correspondence to the simulated data at low d . For larger d a small deviation arises (compare legends of Fig. 3(a) and (b)). However, for the films relevant for this study d is always small and we therefore neglect this deviation.

III. EXPERIMENTS AND DISCUSSION

A. Quantifying ε_1 of thin films

Experimentally we tested our method on several thin-film samples, which were deposited directly on top of the resonator chip, similar to the schematic depiction of Fig. 1(b). The film thickness was characterized after deposition using atomic force microscopy (AFM) on a purposely created edge in the corner of the chip, assuming uniform sample deposition. Microwave data have been acquired using a vector network analyzer (VNA), covering frequencies up to 20 GHz, and either a ^4He cryostat with variable temperature insert (VTI)⁴³ or a ^4He glass bath cryostat⁴⁴ to reach cryogenic temperatures; sample temperature T was 1.7 K unless stated otherwise. This temperature is measured with a Cernox temperature sensor close to the resonators, and we estimate its accuracy to about 20 mK. The output power of the VNA was chosen around -40 dBm to avoid possible regimes of non-linearity at lower powers due to two-level fluctuators⁴⁵ and at higher powers due to the superconductor^{46,47}.

In Fig. 4(a) we plot data obtained for a $6 \mu\text{m}$ thick film of photoresist. While the bare resonator chip features two clear resonances near 5.25 GHz in the transmission spectrum (for two individual resonators), these resonances are shifted to $\approx 5.05 \text{ GHz}$ after deposition of the photoresist.

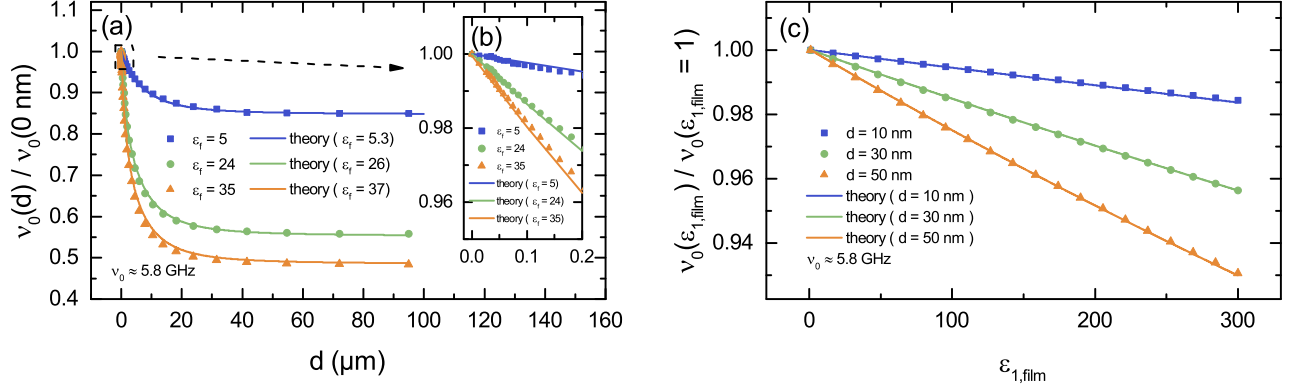


FIG. 3. (a) Normalized resonance frequency $\nu_0(d)/\nu_0(0 \text{ nm})$ of a resonator at about $\nu_0(0 \text{ nm}) \approx 5.8 \text{ GHz}$ as a function of sample layer thickness d . Data points show simulation data, solid lines show theoretical predictions following conformal mapping theory. (b) Enlarged data from (a) in the ultra-thin range up to 200 nm. (c) Normalized resonance frequency $\nu_0(\epsilon_{1, \text{film}})/\nu_0(\epsilon_{1, \text{film}} = 1)$ of a resonator at about $\nu_0(\epsilon_{1, \text{film}} = 1) \approx 5.8 \text{ GHz}$ as a function of $\epsilon_{1, \text{film}}$.

sist. From this 200 MHz shift in resonance frequency we determine ϵ_1 of the film using conformal mapping technique, like presented in Fig. 3. The resulting values are around 2.8-3, which corresponds well with the nominal value of photoresist of about 2.7-3⁴⁸. The slight difference in obtained ϵ_1 between both resonances is attributed to the fact that these resonances belong to two resonators at different locations on the resonator chip. Therefore, the film thickness of the spin-coated photoresist can vary slightly between these two resonators, and consequently the data analysis, assuming the same thickness for both resonators, leads to different ϵ_1 values.

Fig. 4(b) presents the transmission spectra for MgF_2 films, as an example: a resonator chip was covered in three iterations, adding approximately 13 nm, 15 nm, and 7 nm, respectively, of thermally evaporated MgF_2 . With each additional layer, the resonance shifts to lower frequencies, which is consistent with the increasing filling factor q of the MgF_2 in Eq. (2). The resulting values of ϵ_1 are depicted in Fig. 4(c) for two different resonators, at fundamentals around 3.09 GHz and 4.24 GHz, and their respective next higher harmonic, at triple the fundamental frequency. The literature value of about $\epsilon_1 \approx 5$ for single-crystalline MgF_2 ^{49,50} is within the error bars of the ϵ_1 values that we obtain for the 13 nm, whereas we obtain larger ϵ_1 -values for the thicker MgF_2 films. Here we should address more closely the sources of error for the ϵ_1 determination. Firstly, the precision of the measured resonator frequency shift enters, which scales as the inverse of the resonator Q . In our case, the latter is of order 10^4 , similar to comparable coplanar microwave devices with substantial coupling^{21,22,44,51,52}, and thus guarantees the high sensitivity that is needed to detect the influence of the thin film. In Fig. 4(d), the size of the error contribution to ϵ_1 , for the 35 nm case as an example, caused by the Q -related uncertainty is marked as $\Delta\nu_0$. But our main error source for the determination of ϵ_1 is the thickness d of the dielectric film, which directly enters ϵ_1 via Eq. (2). For the thickness determination of each added MgF_2 layer we estimate an error of 3 nm. The resulting error contribution, marked as Δd in Fig. 4(d), clearly dominates the overall error bar for the absolute value of

ϵ_1 . Additional error sources relate to the absolute values of the resonator dimensions S and W , but these are small compared to the error in d .

The third material that we tested as thin film is SiO_2 , which was electron-beam evaporated, with thickness of 50 nm. In Fig. 4(c) we show the obtained ϵ_1 for two resonators, with fundamentals around 2.58 GHz and 3.77 GHz and including additional harmonics. These data are consistent with the $\epsilon_1 \approx 3.9$ for SiO_2 ⁵³.

With these experiments on thin films we demonstrated that our measurement method is sensitive enough to probe dielectric films in the nm-thickness regime. It is possible to determine ϵ_1 of these thin-film samples using conformal mapping techniques.

B. Determining temperature dependence

All data presented so far were obtained at a fixed temperature of 1.7 K. If instead one is interested in temperature-dependent $\epsilon_1(T)$ information on the thin film, one faces the additional challenge that the properties of the superconducting Nb are also temperature dependent. Therefore we designed the resonator chips with in-situ reference resonators. As shown in Fig. 1(d), each resonator has a counterpart with same length l and frequency, which is located on the opposite side of the feedline. With this setup it is possible to probe the thin-film sample with one of the two resonators and leave the other resonator empty and unperturbed, if only one half of the resonator chip is covered by the sample and the other is uncovered. The empty resonator is then only affected by the temperature dependence of the superconducting Nb-layer. Fig. 5(a) shows the normalized resonance frequencies for such a setup, where one resonator is unoccupied and the other is probing a bulk single-crystal SrTiO_3 sample, which was placed on top of part of the chip as schematically shown in the inset of Fig. 5(b). We chose SrTiO_3 as a test sample since it has a well-known pronounced temperature dependence at cryogenic temperatures⁵⁴⁻⁵⁷. Both resonances shift upon increasing the temperature from 1.6 K to 8.5 K,

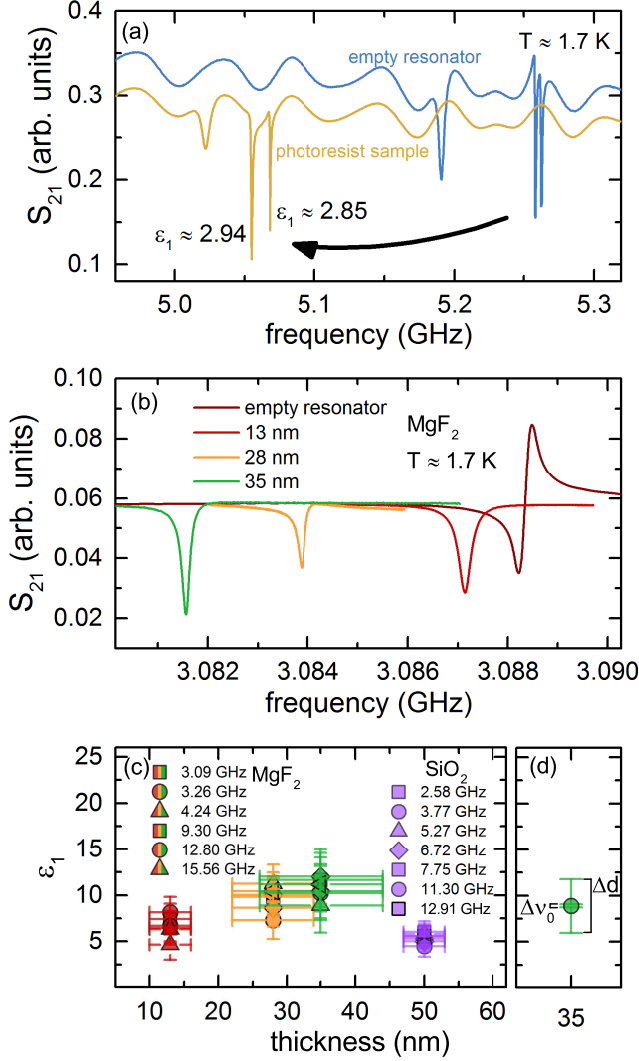


FIG. 4. (a) Spectrum of a resonator chip spin-coated with a 6 μm -thick photoresist layer in comparison to the spectrum of the resonator without sample. The values of ϵ_1 derived from the resonance shift are stated. (b) Spectra of a resonance at about 3.08 GHz for the empty resonator and three different MgF_2 -sample layer thicknesses. With increasing layer thickness the resonance shifts to lower values. (c) ϵ_1 for resonances at different frequencies for MgF_2 and SiO_2 samples. Symbol types show resonances of a single resonator (fundamental and harmonics). (d) ϵ_1 determined with the resonance at 4.24 GHz for the MgF_2 sample of 35 nm thickness shown with detailed y-error bars stemming from multiple error sources.

although in different directions. The resonance of the unoccupied resonator shifts to lower frequencies, since the superconducting penetration depth λ into the Nb increases and the effective resonator volume changes^{42,58}. This can be modeled using the change in impedance Z of the resonator, derived from conformal mapping, and is fitted to the data. Frequency-independent values such as the superconducting London penetration depth λ_0 at zero temperature⁵⁹ (here: $\lambda_0 \approx 609$ nm, comparable to previous studies⁵⁸) and the critical temperature T_c of this particular Nb-resonator (here: $T_c \approx 9.0$ K) are determined. In contrast, the resonance of the resonator under influence of the SrTiO_3 sample shifts to

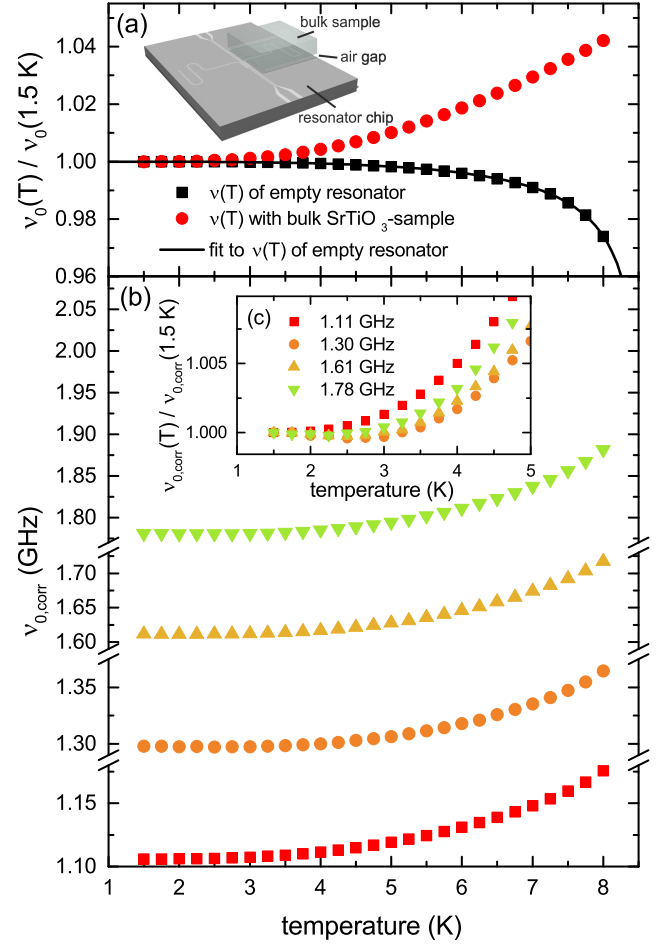


FIG. 5. (a) Resonance frequencies of two resonators, with and without SrTiO_3 sample, measured as function of temperature and normalized to the value at the lowest temperature of 1.5 K. The full line models the temperature dependence of the superconducting Nb. Inset: Schematic view of resonator chip with bulk sample covering one of two resonators. (b) Frequencies of SrTiO_3 -loaded resonator for four modes, with the influence of the superconductor corrected, i.e. with the remaining temperature dependence stemming from $\epsilon_1(T)$ of SrTiO_3 . (c) Data sets of (b), each normalized to the lowest-temperature value.

higher frequencies, which is primarily caused by a reduction in $\epsilon_1(T)$ of the sample but also superimposed by the properties of Nb. With λ_0 and T_c of our Nb the superimposed shift can be eliminated and one obtains a corrected frequency $\nu_{0,\text{corr}}$ with temperature dependence only due to $\epsilon_1(T)$ of SrTiO_3 , which is shown in Fig. 5(b) for four different modes. These data confirm that $\epsilon_1(T)$ of SrTiO_3 is almost constant below 3 K, but decreases strongly for higher temperatures^{55–57}. For better comparison, Fig. 5(c) shows these data normalized to their lowest-temperature values. Here one can identify another, much weaker feature for some of the data sets, namely a faint minimum in $\nu_{0,\text{corr}}(T)$ between 2 and 3 K, corresponding to a maximum in $\epsilon_1(T)$, as previously reported for much lower probing frequencies^{55–57}. Why this minimum in $\nu_{0,\text{corr}}(T)$ is less pronounced for some modes than for others remains to be addressed.

From the data in Fig. 5 one should be able to deter-

mine $\varepsilon_1(T)$ of bulk SrTiO₃, but the procedure equivalent to the case of thin films described above leads to ε_1 values dramatically lower than expected^{54–57,60}. This is due to the placement of the bulk SrTiO₃ sample on top of the resonator chip, as shown in the inset of Fig. 5(a). With this procedure an inevitable air-gap of a few tens of μm between resonator chip and the sample remains. This gap reduces the influence of the sample on the microwave properties and consequently the determined ε_1 is underestimated. For thin films directly deposited onto the dielectric substrate this air-gap problem does not exist.

Conceptually, our measurement method should give access not only to ε_1 of dielectric films, but also to the imaginary part ε_2 , which quantifies microwave loss and affects the resonator Q . However, the thin films of this study have rather low loss, and we did not succeed at this stage to properly quantify their ε_2 . To reach this goal, one has to separate the different loss contributions of the resonators, with main aspects being conduction losses in the Nb, dielectric losses in the substrate and the film under study, and coupling losses to the microwave circuitry. For the present experiments the latter is the most intricate contribution, and here future studies will indicate how sensitive this technique can be to determine the thin-film losses.

IV. CONCLUSIONS

In this study we demonstrated an experimental approach to cryogenic thin-film dielectric measurements. Based on a coplanar microwave waveguide design we determined the dielectric constant ε_1 of sample films in the nm-thickness regime utilizing a resonant waveguide geometry with inductively coupled $\lambda/4$ -resonators. We performed simulations on various resonator parameters in order to establish optimum coupling and enhance sensitivity for thin films. We derived ε_1 from a shift in resonance frequency with conformal mapping by performing simulations in the desired thickness and ε_1 -regime. Experimental data were acquired on several thin-film samples, namely photoresist, MgF₂, and SiO₂ layers in the nm to μm -thickness-regime, and values for ε_1 could be calculated. A temperature-dependent measurement was presented for a SrTiO₃ sample.

From this measurement method a variety of research areas could profit. One particular case is the study of disordered or two-dimensional (weakly) superconducting materials, e.g. granular superconductors^{17,61–63} and materials which feature a superconductor-insulator transition^{18,64,65}. These phenomena only occur at low temperatures, and thus our choice of superconducting resonators as probes does not constitute any restriction in relevant temperatures. If instead one is interested in dielectric films at higher temperatures, then one might consider metallic planar resonators, but the substantially lower resonator Q then immediately leads to reduction of sensitivity by at least two orders of magnitude⁶⁶. Resonators made of high- T_c superconductors thus might also be of interest here⁶⁷.

V. ACKNOWLEDGMENTS

We thank G. Untereiner, M. Ubl, A. Farag and P. Flad for support with sample preparation. Financial support by DFG, in particular SCHE 1580/6, is thankfully acknowledged.

- ¹S. Guha and V. Narayanan, *Annu. Rev. Mater. Res.* **39**, 181 (2009).
- ²L. Martinu and D. Poitras, *J. Vac. Sci. Technol., A* **18**, 2619 (2000).
- ³S. Rogge, D. Natelson, and D. D. Osheroff, *Phys. Rev. Lett.* **76**, 3136 (1996).
- ⁴N. Setter, D. Damjanovic, L. Eng, G. Fox, S. Gevorgian, S. Hong, A. Kingon, H. Kohlstedt, N. Y. Park, G. B. Stephenson, I. Stolitchnov, A. K. Tagansteve, D. V. Taylor, T. Yamada, and S. Streiffer, *J. Appl. Phys.* **100**, 051606 (2006).
- ⁵M. Hering, M. Scheffler, M. Dressel, and H. v. Löhneysen, *Phys. Rev. B* **75**, 205203 (2007).
- ⁶R. Ramesh and N. A. Spaldin, *Nat Mater* **6**, 21 (2007).
- ⁷C. N. Works, *J. Appl. Phys.* **18**, 605 (1947).
- ⁸K. H. Bredeen and J. B. Langley, *Rev. Sci. Instrum.* **40**, 1162 (1969).
- ⁹Y. Yagil, P. Gadenne, C. Julien, and G. Deutscher, *Phys. Rev. B* **46**, 2503 (1992).
- ¹⁰C. Guo, G. Rodriguez, A. Lobad, and A. J. Taylor, *Phys. Rev. Lett.* **84**, 4493 (2000).
- ¹¹M. Hövel, B. Gompf, and M. Dressel, *Phys. Rev. B* **81**, 035402 (2010).
- ¹²J. Krupka, *Meas. Sci. Technol.* **17**, R55 (2006).
- ¹³E. Langereis, S. B. S. Heil, H. C. M. Knoops, W. Keuning, M. C. M. van de Sanden, and W. M. M. Kessels, *J. Phys. D: Appl. Phys.* **42**, 073001 (2009).
- ¹⁴Y. Li, D. Tsui, T. Sajoto, L. Engel, M. Santos, and M. Shayegan, *Solid State Commun.* **95**, 619 (1995).
- ¹⁵A. D. Caviglia, S. Gariglio, N. Reyren, D. Jaccard, T. Schneider, M. Gabay, S. Thiel, G. Hammerl, J. Mannhart, and J. M. Triscone, *Nature* **456**, 624 (2008).
- ¹⁶M. Ovadia, D. Kalok, I. Tamir, S. Mitra, B. Sacepe, and D. Shahar, *Sci Rep* **5**, 13503 (2015).
- ¹⁷U. S. Pracht, N. Bachar, L. Benfatto, G. Deutscher, E. Farber, M. Dressel, and M. Scheffler, *Phys. Rev. B* **93**, 100503 (2016).
- ¹⁸M. V. Feigelman, D. A. Ivanov, and E. Cuevas, *New J. Phys.* **20**, 053045 (2018).
- ¹⁹M. Scheffler, M. Dressel, M. Jourdan, and H. Adrian, *Nature* **438**, 1135 (2005).
- ²⁰M. Scheffler, M. M. Felger, M. Thiemann, D. Hafner, K. Schlegel, M. Dressel, K. S. Ilin, M. Siegel, S. Seiro, C. Geibel, and F. Steglich, *Acta IMEKO* **4**, 47 (2015).
- ²¹L. Frunzio, A. Wallraff, D. Schuster, J. Majer, and R. Schoelkopf, *IEEE Trans. Appl. Supercond.* **15**, 860 (2005).
- ²²M. Göppl, A. Fragner, M. Baur, R. Bianchetti, S. Filipp, J. M. Fink, P. J. Leek, G. Puebla, L. Steffen, and A. Wallraff, *J. Appl. Phys.* **104**, 113904 (2008).
- ²³J. Zmuidzinas, *Annual Review of Condensed Matter Physics* **3**, 169 (2012).
- ²⁴Y. Wiemann, J. Simmendinger, C. Clauss, L. Bogani, D. Bothner, D. Koelle, R. Kleiner, M. Dressel, and M. Scheffler, *Appl. Phys. Lett.* **106**, 193505 (2015).
- ²⁵D. Bothner, T. Gaber, M. Kemmler, D. Koelle, R. Kleiner, S. Wünsch, and M. Siegel, *Phys. Rev. B* **86**, 014517 (2012).
- ²⁶N. G. Ebensperger, M. Thiemann, M. Dressel, and M. Scheffler, *Supercond. Sci. Technol.* **29**, 115004 (2016).
- ²⁷L. Grünhaupt, N. Maleeva, S. T. Skacel, M. Calvo, F. Levy-Bertrand, A. V. Ustinov, H. Rotzinger, A. Monfardini, G. Catealani, and I. M. Pop, *Phys. Rev. Lett.* **121**, 117001 (2018).
- ²⁸A. Wallraff, D. I. Schuster, A. Blais, L. Frunzio, R.-S. Huang, J. Majer, S. Kumar, S. M. Girvin, and R. J. Schoelkopf, *Nature* **431**, 162 (2004).
- ²⁹M. H. Devoret and R. J. Schoelkopf, *Science* **339**, 1169 (2013).
- ³⁰X. Gu, A. F. Kockum, A. Miranowicz, Y.-X. Liu, and F. Nori, *Phys. Rep.* **718-719**, 1 (2017).

- ³¹P. K. Day, H. G. LeDuc, B. A. Mazin, A. Vayonakis, and J. Zmuidzinas, *Nature* **425**, 817 (2003).
- ³²E. S. Battistelli, F. Bellini, C. Bucci, M. Calvo, L. Cardani, N. Casali, M. G. Castellano, I. Colantoni, A. Coppolecchia, C. Cosmelli, A. Cruciani, P. de Bernardis, S. Di Domizio, A. D’Addabbo, M. Martinez, S. Masi, L. Pagnanini, C. Tomei, and M. Vignati, *The European Physical Journal C* **75**, 353 (2015).
- ³³R. Adam, A. Adane, P. A. R. Ade, P. André, A. Andrianasolo, H. Aussel, A. Beelen, A. Benoît, A. Bideaud, N. Billot, O. Bourrion, A. Bracco, M. Calvo, A. Catalano, G. Coiffard, B. Comis, M. De Petris, F.-X. Désert, S. Doyle, E. F. C. Driessen, R. Evans, J. Goupy, C. Kramer, G. Lagache, S. Leclercq, J.-P. Leggeri, J.-F. Lestrade, J. F. Macías-Pérez, P. Mauskopf, F. Mayet, A. Maury, A. Monfardini, S. Navarro, E. Pascale, L. Perotto, G. Pisano, N. Ponthieu, V. Revéret, A. Rigby, A. Ritacco, C. Romero, H. Roussel, F. Ruppig, K. Schuster, A. Sievers, S. Triqueneaux, C. Tucker, and R. Zylka, *Astron. Astrophys.* **609**, A115 (2018).
- ³⁴M. Scheffler, K. Schlegel, C. Clauss, D. Hafner, C. Fella, M. Dressel, M. Jourdan, J. Sichelschmidt, C. Krellner, C. Geibel, and F. Steglich, *physica status solidi (b)* **250**, 439 (2013).
- ³⁵M. Thiemann, M. H. Beutel, M. Dressel, N. R. Lee-Hone, D. M. Broun, E. Fillis-Tsirakis, H. Boschker, J. Mannhart, and M. Scheffler, *Phys. Rev. Lett.* **120**, 237002 (2018).
- ³⁶T. Konaka, M. Sato, H. Asano, and S. Kubo, *J. Supercond.* **4**, 283 (1991).
- ³⁷J. Krupka, R. G. Geyer, M. Kuhn, and J. H. Hinken, *IEEE Trans. Microwave Theory Tech.* **42**, 1886 (1994).
- ³⁸J. Krupka, D. Krzysztof, M. Tobar, J. Hartnett, and R. G. Geyer, *Meas. Sci. Technol.* **10**, 387 (1999).
- ³⁹R. N. Simons, *Coplanar Waveguide Circuits, Components, and Systems* (John Wiley & Sons, Inc., 2001).
- ⁴⁰K. Geerlings, S. Shankar, E. Edwards, L. Frunzio, R. J. Schoelkopf, and M. H. Devoret, *Appl. Phys. Lett.* **100**, 192601 (2012).
- ⁴¹I. Besedin and A. P. Menushenkov, *EPJ Quantum Technology* **5**, 2 (2018).
- ⁴²D. Hafner, M. Dressel, and M. Scheffler, *Rev. Sci. Instrum.* **85**, 014702 (2014).
- ⁴³C. Clauss, D. Bothner, D. Koelle, R. Kleiner, L. Bogani, M. Scheffler, and M. Dressel, *Appl. Phys. Lett.* **102**, 162601 (2013).
- ⁴⁴D. S. Rausch, M. Thiemann, M. Dressel, D. Bothner, D. Koelle, R. Kleiner, and M. Scheffler, *J. Phys. D* **51**, 465301 (2018).
- ⁴⁵A. D. O’Connell, M. Ansmann, R. C. Bialczak, M. Hofheinz, N. Katz, E. Lucero, C. McKenney, M. Neeley, H. Wang, E. M. Weig, A. N. Cleland, and J. M. Martinis, *Appl. Phys. Lett.* **92**, 112903 (2008).
- ⁴⁶C. C. Chin, D. E. Oates, G. Dresselhaus, and M. S. Dresselhaus, *Phys. Rev. B* **45**, 4788 (1992).
- ⁴⁷M. Zinßer, K. Schlegel, M. Dressel, and M. Scheffler, *Rev. Sci. Instrum.* **90**, 034704 (2019).
- ⁴⁸MicroChemicals GmbH, MicroChemicals GmbH, 89079 Ulm, Germany (2019).
- ⁴⁹J. Fontanella, C. Andeen, and D. Schuele, *J. Appl. Phys.* **45**, 2852 (1974).
- ⁵⁰M. V. Jacob, J. Krupka, J. Mazierska, and G. S. Woods, *Materials Science and Engineering: A* **427**, 175 (2006).
- ⁵¹G. Hammer, S. Wuensch, M. Roesch, K. Ilin, E. Crocoll, and M. Siegel, *Supercond. Sci. Technol.* **20**, 408 (2007).
- ⁵²R. Barends, J. J. A. Baselmans, J. N. Hovenier, J. R. Gao, S. J. C. Yates, T. M. Klapwijk, and H. F. C. Hoevers, *IEEE Trans. Appl. Superconduct.* **17**, 263 (2007).
- ⁵³G. Siddall, *Vacuum* **9**, 274 (1959).
- ⁵⁴T. Sakudo and H. Unoki, *Phys. Rev. Lett.* **26**, 851 (1971).
- ⁵⁵K. A. Müller and H. Burkard, *Phys. Rev. B* **19**, 3593 (1979).
- ⁵⁶R. Viana, P. Lunkenheimer, J. Hemberger, R. Böhmer, and A. Loidl, *Phys. Rev. B* **50**, 601 (1994).
- ⁵⁷S. E. Rowley, L. J. Spalek, R. P. Smith, M. P. M. Dean, M. Itoh, J. F. Scott, G. G. Lonzarich, and S. S. Saxena, *Nat. Phys.* **10**, 367 (2014).
- ⁵⁸M. Thiemann, D. Bothner, D. Koelle, R. Kleiner, M. Dressel, and M. Scheffler, *J. Phys. Conf. Ser.* **568**, 022043 (2014).
- ⁵⁹F. London, H. London, and F. A. Lindemann, *Proc. R. Soc. Lond. A* **149**, 71 (1935).
- ⁶⁰D. Davidovikj, N. Manca, H. S. J. van der Zant, A. D. Caviglia, and G. A. Steele, *Phys. Rev. B* **95**, 214513 (2017).
- ⁶¹J. Delahaye, J. Honoré, and T. Grenet, *Phys. Rev. Lett.* **106**, 186602 (2011).
- ⁶²F. Levy-Bertrand, T. Klein, T. Grenet, O. Dupré, A. Benoît, A. Bideaud, O. Bourrion, M. Calvo, A. Catalano, A. Gomez, J. Goupy, L. Grünhaupt, U. v. Luepke, N. Maleeva, F. Valenti, I. M. Pop, and A. Monfardini, *Phys. Rev. B* **99**, 094506 (2019).
- ⁶³M. H. Beutel, N. G. Ebensperger, M. Thiemann, G. Untereiner, V. Fritz, M. Javaheri Rahim, J. Nägele, R. Rösslhuber, M. Dressel, and M. Scheffler, *Supercond. Sci. Technol.* **29**, 085011 (2016).
- ⁶⁴R. Crane, N. P. Armitage, A. Johansson, G. Sambandamurthy, D. Shahar, and G. Grüner, *Phys. Rev. B* **75**, 094506 (2007).
- ⁶⁵M. V. Feigelman, L. B. Ioffe, V. E. Kravtsov, and E. Cuevas, *Ann. Phys.* **325**, 1390 (2010).
- ⁶⁶M. Javaheri Rahim, T. Lehleiter, D. Bothner, C. Krellner, D. Koelle, R. Kleiner, M. Dressel, and M. Scheffler, *J. Phys. D: Appl. Phys.* **49**, 395501 (2016).
- ⁶⁷A. Ghirri, C. Bonizzoni, D. Gerace, S. Sanna, A. Cassinese, and M. Affronte, *Appl. Phys. Lett.* **106**, 184101 (2015).